Assessing the impacts of reservoirs on the downstream flood frequency by coupling the effect of the scheduling-related multivariate rainfall into an indicator of reservoir effects

Bin Xiong[1], Lihua Xiong[1*], Jun Xia[1], Chong-Yu Xu[1, 3], Cong Jiang[2], Tao Du[4]

1. State Key Laboratory of Water Resources and Hydropower Engineering Science, Wuhan University, Wuhan 430072, China

2. School of Environmental Studies, China University of Geosciences, Wuhan 430074, China

3. Department of Geosciences, University of Oslo, P.O. Box 1022 Blindern, N-0315 Oslo, Norway

4. Bureau of Hydrology, Changjiang Water Resources Commission, Wuhan 430010, China

** Corresponding author:*

Lihua Xiong, PhD, Professor

State Key Laboratory of Water Resources and Hydropower Engineering Science

Wuhan University, Wuhan 430072, China

E-mail: xionglh@whu.edu.cn

Telephone: +86-13871078660

Fax: +86-27-68773568

Abstract:

Many studies have shown that the downstream flood regimes have been significantly altered by upstream reservoir operation. Reservoir effects on the downstream flow regime are normally carried out by comparing the pre-dam and post-dam frequencies of some streamflow indicators such as floods and droughts. In this paper, a rainfall-reservoir composite index (RRCI) is developed to precisely quantify reservoir impacts on downstream flood frequency under a framework of the covariate-based nonstationary flood frequency analysis with Bayesian inference method. The RRCI is derived from the combination of both a reservoir index (RI) for measuring the effects of reservoir storage capacity and a rainfall index, i.e., the OR-joint exceedance probability (OR-JEP) of some scheduling-related variables selected out of the five variables describing multiday antecedent rainfall input (MARI), for measuring the effects of antecedent rainfall on reservoir operation. Then, with RI-dependent or RRCI-dependent distribution parameters, five distributions, i.e., Gamma, Weibull, Lognormal, Gumbel and Generalized Extreme Value, are used to analyze the annual maximum daily flow (AMDF) of Ankang, Huangjiagang and Huangzhuang gauging stations of Hanjiang River, China. A phenomenon is observed that although most flood peaks downstream of reservoirs had been reduced in magnitude by the upstream reservoirs, some relatively large flood events still occurred several times, e.g., at the Huangzhuang station in 1983. The results of nonstationary flood frequency analysis show that, in comparison to RI, RRCI that combines both RI and OR-JEP can make a much better explanation for such a phenomenon of the flood occurrences downstream of reservoirs. Bayesian inference of the 100-year return level of AMDF shows that the optimal RRCI-dependent distribution, compared to the RI-dependent one, gives relative smaller estimate values but there exist exceptions due to some low OR-JEP values, and provides a smaller uncertainty range. This study highlights the necessity of including the antecedent rainfall effects, in addition to the effects of reservoir storage capacity, on reservoir operation in assessing the reservoir effects on downstream flood frequency. This analysis might provide a more comprehensive approach for downstream flood risk management under the impacts of reservoirs.

Keywords: Nonstationary flood frequency analysis; downstream floods; reservoir; antecedent rainfall; Bayesian inference; Hanjiang River

1 Introduction

River floods are generated by various complex nonlinear processes involving physical factors including “hydrological pre-conditions (e.g. soil saturation, snow cover), meteorological conditions (e.g. amount, intensity, and spatial and temporal distribution of rainfall), runoff generation processes as well as river routing (e.g. superposition of flood waves in the main river and its tributaries)” (Wyżga et al., 2016). In general, without reservoirs, the flood extremes downstream of most rain-dominated basins are mainly related to the extreme rainfall in the drainage area. However, with reservoirs, the downstream flood regimes should be totally different due to upstream flood control scheduling. In the literature, the significant hydrological alterations caused by reservoirs are demonstrated in the many areas of the world. Graf (1999) showed that the dams have greater effects on the streamflow than the global climate change in America. Benito and Thorndycraft (2005) reported various significant changes of the pre- and post-dam hydrologic regimes (e.g., minimum and maximum flows over different durations) across the United States. Batalla et al. (2004) demonstrated an evident reservoir-induced hydrologic alteration in the North-Eastern Spain. Yang et al. (2008) indicated the spatial variability of the hydrological regimes alteration caused by the reservoirs in the middle and lower Yellow River, China. Mei et al. (2015) found that the Three Gorges Dam, the largest dam in the world, has significantly changed the downstream hydrological regimes. In recent years, the cause-effect mechanisms of the downstream flood peak reduction were also investigated in some literature (Ayalew et al., 2013; 2015; Volpi et al., 2018). For example, Volpi et al. (2018) suggested that for a single reservoir, the downstream flood peak reduction is mainly dependent on its position along the river, its spillway and its storage capacity based on a parsimonious instantaneous unit hydrograph-based model. These studies have revealed that it is crucial to assess the impacts of reservoirs on downstream flood regimes for the success of downstream flood risk management.

Flood frequency analysis is the most common technique used by hydrologists to gain knowledge of flood regimes. For conventional or stationary frequency analysis, a basic hypothesis is that hydrologic time series keeps stationarity, i.e., “free of trends, shifts or periodicity (cyclicity)” (Salas, 1993). However, in many cases, the change of flood regime has demonstrated that this strict assumption is invalid (Kwon et al., 2008; Milly et al., 2008). Nonstationarity in the flood regime downstream of dams makes frequency analysis more complicate. Actually, the frequency of floods downstream of dams is closely related to upstream flood operation. In recent years, there are a lot of attempts linking flood generating mechanisms and reservoir operation to the frequency of downstream floods (Gilroy and Mccuen, 2012; Goel et al., 1997; Lee et al., 2017; Liang et al., 2017; Su and Chen, 2018; Yan et al., 2017).

Previous studies have meaningfully increased the knowledge about the reservoir-induced nonstationarity of downstream hydrological extreme frequency (Ayalew et al., 2013; López and Francés, 2013; Liang et al., 2017; Magilligan and Nislow, 2005; Su and Chen, 2018; Wang et al., 2017; Zhang et al., 2015). There are two main approaches to incorporate reservoir effects into flood frequency analysis: the hydrological model simulation approach and the nonstationary frequency modeling approach. In the first approach, the regulated flood time series can be simulated by using three model components, i.e., the stochastic rainfall generator, the rainfall-runoff model and the reservoir flood operation module which includes the reservoir storage capacity, the size of release structures and the operation rules. The continuous simulation method can explicitly account for the reservoir effects on flood in the hypothetical case. However, it is difficult to apply this approach to the most real cases (Volpi et al., 2018), because the simplifying assumptions of this approach are just satisfied in a few of basins with single small reservoir. Furthermore, even if the basins meet the simplifying assumptions, the detailed information required in this approach are probably unavailable. Thus, our attention is focused on the second method, the nonstationary frequency modeling approach. Nonstationary distribution models have been widely used to deal with the nonstationarity of extreme values series. In nonstationary distribution models, distribution parameters are expressed as the functions of covariates to determine the conditional distributions of the extreme values series. According to extreme value theory, the maxima series can generally be described by the Generalized Extreme Value distribution (GEV). Thus, previous studies (Adlouni et al., 2007; Ouarda and El‐Adlouni, 2011) have used the nonstationary Generalized Extreme Value distribution to describe nonstationary maxima series. Scarf (1992) modeled the change in the location and scale parameters of GEV over time through the power function relationship. Coles (2001) introduced several time-dependent structures (e.g., trend, quadratic and change-point) into the location, scale and shape parameters of GEV. Adlouni et al. (2007) provided a general nonstationary GEV model with an improved parameter estimate method. In recent years, “generalized additive models for location, scale and shape” (GAMLSS) was widely used in nonstationary hydrological frequency analysis (Du et al., 2015; Jiang et al., 2014; López and Francés, 2013; Rigby and Stasinopoulos, 2005; Villarini et al., 2009). GAMLSS provides various candidate distributions for frequency analysis, e.g., Weibull, Gamma, Gumbel, and Lognormal distributions. However, GEV is rarely involved in the candidate distributions of GAMLSS. In terms of the parameter estimation method for the nonstationary distribution model, the maximum likelihood (ML) method is the most common parameter estimate method. However, the ML method for the nonstationary distribution model may diverge when using numerical techniques to solve the likelihood function with the small sample. Another drawback of the ML method is its inconvenience to describe the uncertainty of model parameters estimates, because the ML can only get one estimate of the model parameters through maximization of the likelihood function. Adlouni et al. (2007) developed the generalized maximum likelihood (GML) method and demonstrated that the GML method has better performance than the ML method in all their cases. Ouarda and El‐Adlouni (2011) introduced the Bayesian nonstationary frequency analysis. The Bayesian inference can get multiple estimates, forming a posterior distribution of model parameters. Thus, the Bayesian method is able to conveniently describe the uncertainty of flood estimates associated with the uncertainty of model parameters.

In the nonstationary frequency modeling approach, a dimensionless reservoir index (RI), as an indicator of reservoir effects, was proposed by López and Francés (2013), and it generally is used as covariate for the expression of the distribution parameters (e.g., location parameter) (Jiang et al., 2014; López and Francés, 2013). Liang et al. (2017) modified the reservoir index by replacing the mean annual runoff in the expression of RI with the annual runoff, so that the modified reservoir index can reflect the impact of reservoirs on downstream flood extremes under different total inflow conditions each year. However, the precision and accuracy in the quantitative analysis of the reservoir effects on the downstream floods need to be improved further.. In fact, the effects of reservoirs may be closely related not only to the static reservoir storage capacity, but also to the dynamic reservoir operation associated with the multiple characteristics (e.g., the peak, the intensity and the total volume) of the multiday antecedent rainfall input (MARI), not just annual runoff.

Therefore, the aim of the study is to develop an indicator named the rainfall-reservoir composite index (RRIC) combining the effects of reservoir storage capacity and MARI on reservoir operation, and then to utilize this indicator as covariate to assess the reservoir effects on the downstream flood frequency. The specific objectives of this study are: (1) to develop RRCI; (2) to compare RRCI with RI through the covariate-based nonstationary flood frequency analysis; and (3) to obtain the downstream flood estimation and its uncertainty based on the optimal nonstationary distribution with Bayesian inference.

2 Methods

To quantify the effects of reservoirs on the frequency of the annual maximum daily flow series (AMDF) downstream of reservoirs, a three-step framework (Figure 1), termed the covariate-based flood frequency analysis using RRIC as covariate, is established. In this section, the methods in this framework are introduced. First, a reservoir index (RI) is defined with additionally considering the effects of reservoir sediment deposition on the storage capacity. Second, RRCI is developed through combining RI and a rainfall index. And then, the C-vine copula model is used to construct to calculate the rainfall index. Fourth and last, the nonstationary distribution models with the Bayesian estimation are clarified.

<Figure 1>

2.1 Reservoir index (RI)

Intuitively, the larger the reservoir capacity relative to the flow of a downstream gauging station, the greater the effects of reservoir on the streamflow regime are possible. To quantify the reservoir-induced alteration to the downstream streamflow regime, Batalla et al. (2004) proposed the impounded runoff index (IRI), a ratio of reservoir capacity (RC) to (unimpaired) mean annual runoff ($\bar{Q}$) at the gauge station, indicated as $\mathrm{IRI} = \mathrm{RC}/\bar{Q}$. For single reservoir, the IRI is a good indicator of the extent to which the reservoir alters streamflow. To analyze the effects of multi-reservoir system on the downsream flood frequency, López and Francés (2013) proposed a dimensionless reservoir index. In this study, we additionally consider the effects of reservoir sediment deposition on the reservoir capacity. Following López and Francés (2013),the reservoir index (RI) for a downstream gauging station is defined as

$$\mathrm{RI} = \sum_{i=1}^{N} \left(\frac{A_i}{A_T} \right) \cdot \left(\frac{\left(1 - \mathrm{LR}_i\right) \cdot \mathrm{RC}_i}{\bar{Q}} \right) \tag{1}$$

where N is the total number of reservoirs upstream of the gauge station, A_i is the total basin area upstream of the i-th reservoir, A_T is the total basin area upstream of the gauge station, RC_i is the total storage capacity of the *i*-th reservoir, LR_i is the loss rate (%) of RC_i due to the sediment deposition (Appendix A). The Eq. (1) indicates that for the reservoir system consisting of small and middle sized reservoirs, RI for the downstream gauging station is generally less than 1, but for the system with some large reservoirs, e.g., multi-year regulating storage reservoirs, RI of the downstream gauging station near this system may be close to 1 or higher.

2.2 Rainfall-reservoir composite index (RRCI)

In addition to the reservoir capacity, multiday antecedent rainfall input (MARI), i.e., an event of the continuous multi-day multivariate rainfall forming the inflow event which will be regulated to become downstream extreme flow by the reservoir system is a key constraint for the scheduling of the reservoir system. In this study, to add the antecedent rainfall effects into the new indicator of reservoir effects, the five variables are considered to describe MARI, i.e., the maximum M (the maximum of daily rainfall in MARI), the intensity I (the mean of daily rainfall in MARI), the volume V (the total of daily rainfall in MARI), the timing T (the end time of MARI in the year) and the distance L (the distance between the rainfall center and the outlet). The reason that M, I, V, and L are selected is that these variables will determine the peak, the total volume and the peak appearance time of the inflow event. The variable T is utilized to capture the information of the remaining storage capacity, due to the staged operation strategies in the flood season for some reservoirs. For the operation strategy of increasing flood limit water level in stages, it is expected that if the timing of MARI is near the end of flood season, the downstream AMDF will be less affected by reservoirs, because of less remaining capacity in this period. Those MARI variables which are selected to construct the new indicator are referred to as the scheduling-related MARI variables (denoted as $X_1, X_2, \ldots, X_d$), hereafter. The extraction procedure of the MARI is detailed in the section 3.2.

We propose the new index called rainfall-reservoir composite index (RRIC) for more comprehensively assessing effects of reservoirs on floods by incorporating the effects of MARI, defined as

$$\mathrm{RRCI} = \begin{cases} \left(P_{\mathrm{MARI}}^{\vee} \left(\bigcup_{i=1}^{d} \left(X_i > x_i \right) \right) \right)^{(1/\mathrm{RI}-1)}, 0 < \mathrm{RI} \le 1 \\ \mathrm{RI}, \mathrm{RI} > 1 \end{cases} \tag{2}$$

where $P_{\mathrm{MARI}}^{\vee}$ is the OR-joint exceedance probability (OR-JEP), i.e., the probability that any one of the given set of values ($x_1, x_2, \ldots, x_d$) for the scheduling-related MARI variables will be exceeded. Here, OR-JEP acts as the rainfall index of measuring the MARI effects. The lower this probability, the greater effects on reservoir operation the MARI has, and then, it is expected that the downstream floods possibly obtain relative large values, and vice versa. Figure 2 illustrates the relationship in the Eq. (2), which shows that RRCI is conditional on both OR-JEP and RI. The Eq. (2) can be expressed as

$$\mathrm{RRCI} = \begin{cases} \left(1 - F\left(x_1, x_2, \ldots x_d\right)\right)^{(1/\mathrm{RI}-1)}, 0 < \mathrm{RI} \le 1 \\ \mathrm{RI}, \mathrm{RI} > 1 \end{cases} \tag{3}$$

where $F(\cdot)$ is the cumulative distribution function (CDF), determining the dependence relationship of the variables. The expectation of RRCI is as follow

$$E(\mathrm{RRCI}) = \int_{\mathbb{R}^d} \left(1 - F\left(x_1, x_2, \ldots x_d\right)\right)^{(1/\mathrm{RI}-1)} dF\left(x_1, x_2, \ldots x_d\right) = \mathrm{RI} \tag{4}$$

In addition, for the OR case, we have

$$P^{\vee}_{\mathrm{MARI}}\left(\bigcup_{i=1}^{d}\left(X_i > x_i\right)\right) \geq P^{\vee}_{\mathrm{MARI}}\left(X_i > x_i\right) \tag{5}$$

The Eq. (3) and Eq. (5) indicate that in addition to RI, RRCI is related to the number and the dependence relationship of the scheduling-related MARI variables. To give a reasonable RRCI, the unrelated MARI variables should not be incorporated. In this study, the number of MARI variables to be incorporated is no more than four to avoid "dimension disaster" in modeling their dependence. To select the scheduling-related MARI variables, the three-step selection procedure includes (1) selecting four variables from the five MARI variables through testing the significance of the Pearson correlation between the MARI variables and AMDF, (2) calculating RRCI for all the possible subsets of the four variables through the *d*-dimensional ($d = 1, 2, 3, 4$) copulas, and (3) identifying the variables through the highest rank correlation coefficient between RRCI and AMDF. The construction method of *d*-dimensional ($d = 2, 3, 4$) distribution $F\left(x_1, x_2, \ldots, x_d\right)$ is described in the following subsection.

<Figure 2>

2.3 C-vine Copula model

In this subsection, a c-vine Copula model for the construction of continuous d-dimensional distribution $F(x_1, x_2, ..., x_d)$ is clarified. The Sklar's theorem (Sklar, 1959) showed that for a continuous d-dimensional distribution, one-dimensional marginals and dependence structure can be separated, and the dependence can be represented by a copula formula as follows

$$F(x_1, x_2, ...x_d | \boldsymbol{\theta}) = C(u_1, u_2, ..., u_d | \boldsymbol{\theta}_c), u_i = F_{X_i}(x_i | \boldsymbol{\theta}_i) \quad (6)$$

where u_i is the univariate marginal distribution of X_i; $C(\cdot)$ is the copula function. $\boldsymbol{\theta}_c$ is the copula parameter vector; $\boldsymbol{\theta}_i$ is the parameter vector of the i-th marginal distribution. $\boldsymbol{\theta} = (\boldsymbol{\theta}_c, \boldsymbol{\theta}_1, \boldsymbol{\theta}_2, ..., \boldsymbol{\theta}_d)$ is the parameter vector of the whole n-dimensional distribution. Thus, the construction of $F(x_1, x_2, ...x_d)$ can be separated into two steps: first is the modeling of the univariate marginals; second is the modeling of the dependence structure. For the first step, we use the empirical distribution as univariate marginal distributions and the change-points of the variables are tested by the Pettitt test (Pettitt, 1979), and then, if any, the marginal with the change-point will be addressed by the estimation method (Xiong et al., 2015). Then, for the second step, the copula construction for the dependence modeling is based on the pair-copula construction method which has been widely used in the previous research (Aas et al., 2009; Xiong et al., 2015). According to Aas et al. (2009), the joint density function $f(x_1, x_2, ..., x_d)$ is written as

$$f\left(x_1, x_2, ..., x_d \middle| \boldsymbol{\theta}\right) = c_{1...n}\left(u_1, u_2, ..., u_d \middle| \boldsymbol{\theta}_c\right) \prod_{i=1}^{d} f_{X_i}\left(x_i \middle| \boldsymbol{\theta}_i\right), u_i = F_{X_i}\left(x_i \middle| \boldsymbol{\theta}_i\right) \tag{7}$$

and the n-dimensional copula density $c_{1...d}\left(u_1, u_2, ..., u_d\right)$, which can be decomposed into $d(d-1)/2$ bivariate copulas, corresponding to a c-vine structure, is given by

$$c_{1...d}\left(u_1, u_2, ..., u_d \middle| \boldsymbol{\theta}_c\right) = \prod_{j=1}^{d-1} \prod_{i=1}^{d-j} c_{j,i+j|1,...,j-1}\left(F\left(u_j \middle| u_1, ..., u_{j-1}\right), F\left(u_{i+j} \middle| u_1, ..., u_{j-1}\right) \middle| \boldsymbol{\theta}_{j,i|1,...,j-1}\right) \tag{8}$$

where $c_{j,i+j|1,...,j-1}$ is the density function of a bivariate pair copula and $\boldsymbol{\theta}_{j,i|1,...,j-1}$ is a parameter vector of the corresponding bivariate pair copula. And the marginal conditional distribution is

$$\begin{aligned} & F\left(u_{i+j} \middle| u_1, ..., u_{j-1}\right) = \\ & \frac{\partial C_{i+j,j-1|1,...,j-2}\left(F\left(u_{i+j} \middle| u_1, ..., u_{j-2}\right), F\left(u_{j-1} \middle| u_1, ..., u_{j-2}\right) \middle| \boldsymbol{\theta}_{i+j,j-1|u_1,...,u_{j-2}}\right)}{\partial F\left(u_{j-1} \middle| u_1, ..., u_{j-2}\right)}, \\ & j = 2, ..., d-1;\ i = 0, ..., n-j \end{aligned} \tag{9}$$

where $C_{i+j,j-1|1,...,j-2}$ is a bivariate copula distribution function. The maximum dimensionality covered in this study is four. Thus for the four-dimensional copula (of which the decomposition is shown in Figure 3), the general expression of Eq. (8) is

$$\begin{aligned} & c_{1234}\left(u_1, u_2, u_3, u_4 \middle| \boldsymbol{\theta}_c\right) = c_{12}\left(u_1, u_2 \middle| \boldsymbol{\theta}_{12}\right) c_{13}\left(u_1, u_3 \middle| \boldsymbol{\theta}_{13}\right) c_{14}\left(u_1, u_4 \middle| \boldsymbol{\theta}_{14}\right) \cdot \\ & c_{23|1}\left(F\left(u_2 \middle| u_1\right), F\left(u_2 \middle| u_1\right) \middle| \boldsymbol{\theta}_{23|1}\right) c_{24|1}\left(F\left(u_2 \middle| u_1\right), F\left(u_4 \middle| u_1\right) \middle| \boldsymbol{\theta}_{24|1}\right) \cdot \\ & c_{34|12}\left(F\left(u_3 \middle| u_1, u_2\right), F\left(u_4 \middle| u_1, u_2\right) \middle| \boldsymbol{\theta}_{34|1}\right) \end{aligned} \tag{10}$$

<Figure 3>

2.4 Covariate-based nonstationary frequency analysis with Bayesian estimation

The covariate-based extreme frequency analysis has been widely used (Villarini et al., 2009; Ouarda and El‐Adlouni, 2011; López and Francés, 2013; Xiong et al., 2018). Following these studies, five distributions, i.e., Gamma (GA), Weibull (WEI), Lognormal (LOGNO), Gumbel (GU) and Generalized Extreme Value (GEV), are used as candidate distributions in this study. And their density functions, the corresponding moments and the used link functions are shown in Table 1. In the following, the nonstationary distribution models based on Bayesian estimation are developed for covariate-based flood frequency analysis.

<Table 1>

Suppose that flood variable Y_t obeys distribution $f_{Y_t}\left(y_t \middle| \boldsymbol{\eta}_t\right)$ with the distribution parameters $\boldsymbol{\eta}_t = \left[\mu_t, \sigma_t, \xi\right]$. In this study, only distribution parameters μ_t and σ_t are allowed to be dependent on covariates, with considering that the shape parameter ξ of GEV is sensitive to quantile estimation of rare events. According to the linear additive formulation of Generalized Additive Models for Location, Scale, and Shape (GAMLSS) (Rigby and Stasinopoulos, 2005; Villarini et al., 2009), seven nonstationary scenarios for the formulas of the two distribution parameters μ_t and σ_t are investigated, as shown in Table 2. The constant scenario (S0) includes one scenario (both μ_t and σ_t are constants). The RI-dependent scenarios (S1) include three scenarios, i.e., S11 (μ_t is RI-dependent and σ_t is constant), S12 (μ_t is constant and σ_t is RI-dependent) and S13 (both μ_t and σ_t are RI-dependent). And the RRCI-dependent scenarios (S2) include S21, S22 and S23 as similar as S11, S12 and S13, respectively.

<Table 2>

In the following, Bayesian inference is introduced. Take GEV_S23 (representing the nonstationary GEV distribution with the S23 scenario) model as an example, the model parameter vector $\boldsymbol{\theta}_{\mathrm{GEV\_S23}} = [\alpha_0, \alpha_1, \beta_0, \beta_1, \xi]$ is to be estimate. We use the Bayesian method to estimate $\boldsymbol{\theta}_{\mathrm{GEV\_S23}}$. Let the prior probability distribution be $\pi\left(\boldsymbol{\theta}_{\mathrm{GEV\_S23}}\right)$ and observations $\boldsymbol{D}$ have the likelihood $l\left(\boldsymbol{D} \middle| \boldsymbol{\theta}_{\mathrm{GEV\_S23}}\right)$, then the posterior probability distribution $p\left(\boldsymbol{\theta}_{\mathrm{GEV\_S23}} \middle| \boldsymbol{D}\right)$ can be calculated with Bayes' theorem, as follow

$$p\left(\boldsymbol{\theta}_{\mathrm{GEV\_S23}} \middle| \boldsymbol{D}\right) = \frac{l\left(\boldsymbol{D} \middle| \boldsymbol{\theta}_{\mathrm{GEV\_S23}}\right) \pi\left(\boldsymbol{\theta}_{\mathrm{GEV\_S23}}\right)}{\int_{\boldsymbol{\Omega}} l\left(\boldsymbol{D} \middle| \boldsymbol{\theta}_{\mathrm{GEV\_S23}}\right) \pi\left(\boldsymbol{\theta}_{\mathrm{GEV\_S23}}\right) d\boldsymbol{\theta}_{\mathrm{GEV\_S23}}} \propto l\left(\boldsymbol{D} \middle| \boldsymbol{\theta}_{\mathrm{GEV\_S23}}\right) \pi\left(\boldsymbol{\theta}_{\mathrm{GEV\_S23}}\right) \tag{11}$$

where the integral is the normalizing constant and $\boldsymbol{\Omega}$ is the whole parameter space. The obvious difference between the Bayesian method and the frequentist method is that the Bayesian method considers the parameters $\boldsymbol{\theta}_{\mathrm{GEV\_S23}}$ to be random variables, and the desired distribution of the random variables can be obtained by a Markov chain which can constructed by using various Markov chain Monte Carlo (MCMC) algorithms (Reis Jr and Stedinger, 2005; Ribatet et al., 2007) to process Eq. (11). And in this study, we use the Metropolis-Hastings algorithm (Chib and Greenberg, 1995; Viglione et al., 2013), which can be done by aid of the R package “MHadaptive” (Chivers, 2012). We use a beta distribution function with the parameters $u = 6$ and $v = 9$, which is suggested by Martins and Stedinger (2000); Martins and Stedinger (2001), as the prior distribution on the shape parameter ξ. For the other model parameters $\alpha_0, \alpha_1, \beta_0, \beta_1$, the prior distributions are set to non-informative (flat) priors. There are two advantage of the Bayesian method. First, as noted by Adlouni et al. (2007), this method allows the addition of the other information, e.g., historical and regional information, through defining the prior distribution. Second, the Bayesian method can provide an explicit way to account for the uncertainty of parameters estimates. In nonstationary case, in the *t*-year, the 95% credible interval for the estimation of the flood quantile corresponding to a given probability p can be obtained from a set of stable parameters estimations $\hat{\boldsymbol{\theta}}^{i}_{\mathrm{GEV\_S23}}(i = 1, 2, ..., M_c)$ in which M_c is the length of the Markov chain.

The procedure of model selection can identify which of the five distributions is optimal, which of the seven nonstationary scenarios is optimal. If all the distribution parameters are identified as constants (S0), this process will be the stationary frequency analysis. To select the optimal model, the Schwarz Bayesian criterion (SBC) (Schwarz, 1978) for each fitted model object is calculated by

$$\mathrm{SBC} = -2\ln\left(\hat{l}\right) + \ln\left(n\right) * \mathrm{df} \tag{12}$$

where $\ln\left(\hat{l}\right)$ is the maximized log-likelihood of the model object, df is the freedom degree and n is the number of data points. SBC has a larger penalty on the over-fitting phenomenon than Akaike information criterion (AIC) (Akaike, 1974). The model object with the lower SBC is preferred. The worm plot and the QQ plot are employed to check whether the model can well represent the data.

3 Study area and data

3.1 Study area

Hanjiang River (Figure 4), with the coordinates of 30°30′-34°30′ N, 106°00′-114°00′ E and a catchment area of 159000 km^2, is the largest tributary of the Yangtze River, China. This area has a warm temperate, semi-humid, continental monsoon climate. The temperature in the basin is not much different from upstream to downstream. Although the elevation range of the study area is quite wide (13–3493 m), the study area is a rainfall-dominated area and the snowmelt contribution is quite limited. Take Ankang gauging station as an example. The timing of AMDF is mainly during the major rainfall period from June to September (Figure S3a, c and d). And the winter is warm with the mean temperature values of more than 2 ℃ as shown in Figure S3b. Since 1960, many reservoirs have been completed in Hanjiang basin. The information of the five major reservoirs has been shown in Table 3, including the longitude, latitude, control area, time for completion and capability. The Danjiangkou Reservoir in central China's Hubei province is the largest one in this basin, and was completed by 1967. As a multi-purpose reservoir, it mainly aims to supply water and control floods, and is also used for electricity generation and irrigation. The reservoir has the total storage capacity of 21.0 billion m^3, the dead storage capacity of 7.23 billion m^3, the effective storage capacity of 10.2 billion m^3, and the flood control capacity of 7.72 billion m^3. After the Danjiangkou Dam Extension Project in 2010, the

Danjiangkou Reservoir gained an additional capacity of 13.0 billion m^3 and an extra flood control storage capacity of 3.3 billion m^3. Besides, this reservoir is operated by the strategy of staged increasing flood limit water level in the flood control season (Zhang et al., 2009).

<Figure 4>

<Table 3>

3.2 Data

The assessment analysis of reservoir effects on flood frequency utilizes the streamflow data, the reservoir data, and the rainfall data. The annual maximum daily flood series (AMDF) is extracted from the daily streamflow records of the three gauges in Hanjiang River basin, namely Ankang (AK) station with a drainage area of 38600 km^2, Huangjiagang (HJG) station with a drainage area of 90491 km^2 and Huangzhuang (HZ) station with a drainage area of 142056 km^2. The streamflow and reservoir data are provided by the Hydrology Bureau of the Changjiang Water Resources Commission, China (http://www.cjh.com.cn/en/index.html). The annual series of the maximum (M), the intensity (I), volume (V), the timing (T) and the distance (L) are extracted from the daily streamflow data to describe the MARI. Note that the timing of MARI is equal to the occurrence time of AMDF in the year, MARI is an areal-averaged event, and any two consecutive days of areal rainfall values in MARI require more than 0.2 mm. Daily areal rainfall is calculated using the inverse distance weighting (IDW) method, based on the rainfall records of 16 stations (shown in Figure 4). These rainfall data are downloaded from the National Climate Center of the China Meteorological Administration (source: http://www.cma.gov.cn/). For AK and HZ gauging stations, all records are available from 1956 to 2015, while the records of HJG gauging station are available from 1956 to 2013.

4 Results and discussion

4.1 Identification of reservoir effects

In order to confirm the impact of reservoirs on annual maximum daily flow (AMDF) in the study area, the mean and standard deviation of AMDF before and after the construction of the two large reservoirs, i.e., the Danjiangkou reservoir (1967) upstream of HJG and HZ stations and the Ankang reservoir (1992) upstream of AK, HJG and HZ stations, are compared. According to the Table 4, the mean and standard deviation of AMDF in AK, HJG and HZ stations has been significantly reduced. Taking the HJG station as an example, the mean of AMDF (1992-2013) is 4139 m^3/s, which is only 0.28 time of 14951 m^3/s (1956-1966) and the standard deviation is 4074 m^3/s, about 0.52 time of 7896 m^3/s (1956-1966).

<Table 4>

Figure 5 presents the linear correlation between the five MARI variables (i.e., the maximum, M; the intensity, I; volume, V; the timing, T; and the distance L) and AMDF. It is found that for M, I, V and T , except for T in AK station, the Pearson correlation coefficients between those four variables and AMDF range from 0.27 to 0.71 (p-value>0.05), indicating that those four variables are significantly related to AMDF. However, there is a Pearson correlation coefficient of no more than 0.24 between *L* and AMDF for each stations, indicating that the location of rainfall may not be significantly related to AMDF of the outlet. Thus, *L* is excluded for the calculation of RRCI. The further analysis for the reservoir effects on downstream AMDF is performed in the following sections.

<Figure 5>

4.2 Results for rainfall-reservoir composite index (RRCI)

To obtain the annual values of RRCI, RI is estimated firstly. RI is affected by the loss of the reservoir capacity but not too much (Figure S2), because the main reservoirs (i.e., Dangjiangkou and Ankang reservoirs) have a small loss rate no more than 15% (Table S1 and Figure S1).

The C-vine copula model is applied to calculate OR-JEP of the scheduling-related MARI variables. In the modeling of the univariate marginal, the marginals of the intensity (*I*) of AK and HJG stations and the volume (*V*) of the HJG station are revised to deal with their significant change-points (Table S2). To identify the scheduling-related variables from *M*, *I*, *V*, and *T*, RRCI for all the possible subsets of *M*, *I*, *V*, and *T* is calculated and compared. The Pearson, Kendall, and Spearman correlation coefficients between RRCI and AMDF are listed in Table 5.Note that the whole decomposition structure of the C-vine copula for each RRCI of the same station is determined by the ordering of the variables of each subset (shown in the cells of the first column of Table 5). Figure 3 is an example for the decomposition structure of the 4-dimensional copula. As shown in the first row of Table 5, there is a negative correlation between AMDF and RI for each station. The values of the Pearson correlation coefficients between AMDF and RI for AK, HJG and HZ stations are -0.37, -0.55 and -0.53, respectively, demonstrating that there is a significant relation between the reservoirs storage capacity and the reduction of AMDF. For each station, except for RRCI of one-dimensional case, the values of the Pearson, Kendall, and Spearman correlation coefficients between RRCI and AMDF are higher than between RI and AMDF. According to the highest Kendall correlation, the scheduling-related variables for the AK station are *M*, *I*, *V* and *T*; those for the HJG station are *I* and *T*; and those for the HZ station are *I*, *V* and *T*.

<Table 5>

Table 6 is the results of copula modeling of the scheduling-related variables, by aid of the R package "VineCopula" (https://CRAN.R-project.org/package=VineCopula). Note that for each bivariate pair in the third column of Table 6, three one-parameter bivariate Archimedean copula families (i.e., the Gumbel, Frank, and Clayton copulas) (Nelsen, 2006), are used to select from. As shown in Table 6, the results of the Cramer-von Mises test (Genest et al., 2009) show that all the C-vine copula models pass the test at the significant level of 0.05, indicating these models are effective for simulating the joint distribution of the scheduling-related variables for three stations. Finally, the variation of RI and RRCI over time is displayed in Figure 6. It is found that for each station, after reservoir construction, in most cases, the annual values of RRCI are larger (close to 1) than those of RI. On the other hand, in few cases, e.g., in 1983 at HZ and HJG stations, the RRCI values are lower than the RI values.

<Figure 6>

<Table 6>

4.3 Flood frequency analysis

In this section, nonstationary flood frequency analysis using RRCI or RI as covariate is performed to investigate how reservoirs affect the downstream flood frequency. The summary of results of fitting the nonstationary models to the flood data is shown in Table 7. Based on SBC, the lowest values indicate that the best models for AK, HJG and HZ stations are the nonstationary WEI distribution with S23, the nonstationary GA distribution with S21, and the nonstationary WEI distribution with S21, hereafter referred to as WEI_S23, GA_S21, WEI_S21, respectively. Note that for any one of the five distributions (i.e., GA, WEI, LOGNO, GU and GEV), the RRCI-dependent scenario has a lower SBC value than the RI-dependent scenario for each gauging station. Furthermore, for the RI-dependent and RRCI-dependent scenarios, taking the HZ station as an example, the optimal formulas of two distribution parameters μ_t and σ_t are given as follows:

(1) WEI_S11

$$\begin{aligned} \mu_t &= \exp\left(9.94 - 2.79\mathrm{RI}\right) \\ \sigma_t &= \exp\left(0.49\right) \end{aligned} \tag{13}$$

(2) WEI_S21

$$\begin{aligned}\mu_t &= \exp\left(9.92 - 1.42\mathrm{RRCI}\right)\\ \sigma_t &= \exp\left(0.73\right)\end{aligned} \tag{14}$$

It is found that in the Eq. (13) and Eq. (14), there are the negative estimates of -2.79 and -1.42 for α_1, respectively, revealing the decreasing degree of the frequency and magnitude of downstream floods due to the reservoir effects.

Figure 7 compares the stationary scenario (S0), the RI-dependent scenario (S1), and the RRCI-dependent scenario (S2) of the same optimal distributions in explaining all the flood values and the several largest flood values for each station. The QQ plots (Figure 7a1, b1 and c1) show that overall, the RRCI-dependent scenario captures more adequately the whole empirical quantiles (particularly the smallest and largest empirical quantiles) than two other scenarios for each station. Furthermore, as shown in Figure 7a2, b2 and c2, for the seven largest floods (observed) of each station, the RRCI-dependent scenario produces lower quantile residuals than two other scenarios.

<Table 7>

<Figure 7>

Figure 8 presents the performance of the best models, i.e., WEI_S23 for AK station, GA_S21 for HJG station and WEI_S21 for HZ station. The points in the worm plots of Figure 8 are within the 95% confidence intervals indicating that the selected models are reasonable. And according to the centile curves plots of Figure 8, the AMFD series is well fitted by the best models. Undoubtedly, with the incorporation of the effects of MARI, the RRCI-dependent scenario well captures the presence of nonstationarity in the downstream flood frequency. Take the case of HZ station (Figure 8c1). After the construction of Danjiangkou Reservoir (1967), due to reservoir operation, most values of AMDF had been reduced in magnitude by this reservoir. However, some relatively large flood events still occurred several times, e.g., 25600 m^3/s in 1983 and 19900 m^3/s in 1975. Obviously, this phenomenon of flood occurrences is well explained by RRCI.

<Figure 8>

The 100-year return levels with the 95% credible interval from WEI_S23 and WEI_S13 for AK station, GA_S21 and GA_S11 for HJG station, and WEI_S21 and WEI_S11 for HZ station are presented in Figure 9. For each station, compared to the optimal RI-dependent distribution, the optimal RRCI-dependent distribution provides a lower 100-year return level but there exist exceptions, and provides a smaller uncertainty range. Besides, after the construction of the main reservoir, the uncertainty range of AK station is larger than HJG and HZ stations. The possible explanation to the larger uncertainty range is that the sample size (1993-2015) of the regulated floods at AK station is smaller, and, furthermore, the dependent relationship between RRCI and AMDF at AK station is weaker.

<Figure 9>

4.4 Discussion

The long-term variation of the AMDF series (Figure 8) indicates that the upstream reservoirs have evidently altered the downstream flood regimes. As an example, since the completion of Danjiangkou reservoir in 1967, the flood magnitude of HZ station is evidently reduced overall. This is consistent with the results on the effects of reservoirs on the hydrological regime of this area in previous literature (Cong et al., 2013; GUO et al., 2008; Jiang et al., 2014; Lu et al., 2009). In this study, it is found that there is a significant difference between those downstream floods affected by the same reservoir system (with the same RI value). In most cases, relative small downstream floods were obtained. However, it is of interest to note that there still occurred unexpected large downstream floods in few cases, in spite of a large RI value. For example, most values of AMDF in HZ station are less 10000 m^3/s since 1967, but the values of AMDF in 1983 and in 1975 are 25600 m^3/s and 19900 m^3/s, respectively. It is highlighted that those unexpected large downstream floods are probably related to the MARI effects on reservoir operation. The five largest (unexpected) floods since 1967 and the corresponding values of the scheduling-related MARI variables in the HZ station are shown in Table 8. It is found that the largest floods of 1967-2015 occurred in 1983. For this flood event, the MARI is a rare event (with the OR-JEP value of 0.435 ranking the second in 1967-2015) due to the largest mean intensity ($I = 20.2\ \text{mm}$) and the second late occurrence ($T = 281$). Surprisingly, all the timing values of the MARI for these five unexpected downstream floods show the high rankings (2-9th). Those timing values are near the end (about the 300th day of the year) of the flood control period (July-October) in this area. Actually, near the end of the major flood control period, the storage capacity able to use should be decreased, because according to the operation rules of Danjiangkou reservoir (Zhang et al., 2009), there is a staged increasing flood limit water level in the flood control season. One important cause for those unexpected large downstream floods is probably that the remaining storage capacity at the end of flood season is not sufficient to reduce some late floods. Therefore, in addition to the own storage capacity of reservoirs, the MARI effects should be indispensably considered when attempting to accurately quantify the reservoir effects on downstream floods.

<Table 8>

With the combination of both RI and OR-JEP, RRCI has a significant difference from RI (Figure 6). With a few exceptions, RRCI values are higher than RI values. It is indicated that the real reservoir impact may be underestimated by RI in most cases. Moreover, RI will also probably overestimate the real reservoir impact in few cases, because of no considering some special rainfall events (i.e., the MARI with low values of OR-JEP). The results of the covariate-based nonstationary flood frequency analysis (Table 7, Figure 7 and Figure 8) demonstrate that compared to the RI-dependent scenario, the RRCI-dependent scenario for the optimal nonstationary distribution more completely captures the presence of nonstationarity in the downstream flood frequency. Therefore, RRCI might be a useful index in accessing the reservoir effects on the downstream flood frequency.

Finally, the estimation errors of OR-JEP should be noted. (1) Only those MARI samples which corresponds to the timing of AMDF are included to estimate OR-JEP; this means that some extreme MARI samples which corresponds to the non-maximum flow are not included, resulting in the estimation error for OR-JEP; to reduce this error, it might be worth considering the use of the peaks-over-threshold sampling method. (2) The areal-averaged MARI is based on the records of 16 rainfall stations with the IDW method; the estimation error of areal-averaged rainfall may be transferred to the OR-JEP estimation error; the additional rainfall site data and spatial distribution information are needed to reduce the OR-JEP estimation error. Nonetheless, the good performance of downstream flood frequency modeling demonstrates the MARI samples still remain representative in this study.

5 Conclusions

Accurately assessing the impact of reservoirs on downstream floods is an important issue for flood risk management. In this study, to evaluate the effects of reservoirs on downstream flood frequency of Hanjiang River, the rainfall-reservoir composite index (RRCI) is derived from the Eq. (2) which takes account of the combination of the reservoir index (RI) and the OR-joint exceedance probability (OR-JEP) of scheduling-related rainfall variables. The main findings are summarized as follows: (1) the magnitude of the downstream flood events has been reduced by the reservoir system in the study area; however, the long-term variation of the observed AMDF series show that despite of the large reservoirs, the unexpected large flood events still occurred several times, e.g., at Huangzhuang station in 1983; and one important cause for the unexpected large floods of Huangzhuang station may be related to the operation strategy of staged increasing flood limit water level for Danjiangkou reservoir. (2) According to the results of the covariate-based nonstationary flood frequency analysis for each station, compared to the optimal RI-dependent distribution, the optimal RRCI-dependent distribution more completely captures the presence of nonstationarity in the downstream flood frequency. (3) Furthermore, in estimating 100-year return level for each station, the optimal RRCI-dependent distribution provides a lower 100-year return level but there exist exceptions, and provides a smaller uncertainty range associated with the uncertainty of model parameter.

Consequently, this study demonstrates the necessity of including the antecedent rainfall effects, in addition to the effects of reservoir storage capacity, on reservoir operation in assessing the reservoir effects on downstream flood frequency. The study might provide a comprehensive approach for the downstream flood risk management under the impacts of reservoirs.

Acknowledgments

This research is financially supported jointly by the National Natural Science Foundation of China (NSFC Grants 41890822 and 51525902), the Research Council of Norway (FRINATEK Project 274310), and the Ministry of Education “111 Project” Fund of China (B18037), all of which are greatly appreciated. We greatly appreciate the editor and the two reviewers for their insightful comments and

constructive suggestions for improving the manuscript. No conflict of interest exists in the submission of the manuscript.

References

Aas, K., Czado, C., Frigessi, A., Bakken, H., 2009. Pair-copula constructions of multiple dependence. Insurance: Mathematics and Economics, 44(2): 182-198. https://doi.org/10.1016/j.insmatheco.2007.02.001

Adlouni, S.E., Ouarda, T.B.M.J., Zhang, X., Roy, R., Bobée, B., 2007. Generalized maximum likelihood estimators for the nonstationary generalized extreme value model. Water Resources Research, 43(3): 455-456. https://doi.org/10.1029/2005WR004545.

Akaike, H., 1974. A new look at the statistical model identification. IEEE Transactions on Automatic Control, 19(6): 716-723. https://doi.org/10.1109/TAC.1974.1100705.

Ayalew, T.B., Krajewski, W.F., Mantilla, R., 2013. Exploring the effect of reservoir storage on peak discharge frequency. Journal of Hydrologic Engineering, 18(12): 1697-1708. https://doi.org/10.1061/(ASCE)HE.1943-5584.0000721.

Ayalew, T.B., Krajewski W.F., Mantilla R., 2015. Insights into Expected Changes in Regulated Flood Frequencies due to the Spatial Configuration of Flood Retention Ponds. Journal of Hydrologic Engineering, 20(10): https://doi.org/10.1061/(ASCE)HE.1943-5584.0001173

Batalla, R.J., Gomez, C.M., Kondolf, G.M., 2004. Reservoir-induced hydrological changes in the Ebro River basin (NE Spain). Journal of Hydrology, 290(1-2): 117-136. https://doi.org/10.1016/j.jhydrol.2003.12.002

Benito, G., Thorndycraft, V.R., 2005. Palaeoflood hydrology and its role in applied hydrological sciences. Journal of Hydrology, 313(1–2): 3-15. https://doi.org/10.1016/j.jhydrol.2005.02.002.

Chib, S., Greenberg, E., 1995. Understanding the metropolis-hastings algorithm. The American Statistician, 49(4): 327-335. https://doi.org/10.1080/00031305.1995.10476177.

Chivers, C., 2012. MHadaptive: General Markov Chain Monte Carlo for Bayesian Inference using adaptive Metropolis-Hastings sampling. https://CRAN.R-project.org/package=MHadaptive

Coles, S., 2001. An introduction to statistical modeling of extreme values. https://doi.org/10.1007/978-1-4471-3675-0

Cong, M., Chunxia, L., Yiqiu, L., 2013. Runoff change in the lower reaches of Ankang Reservoir and the influence of Ankang Reservoir on its downstream. Resources and Environment in the Yangtze Basin, 22(11): 1433-1440.

Du, T. et al., 2015. Return period and risk analysis of nonstationary low-flow series under climate change. Journal of Hydrology, 527: 234-250. https://doi.org/10.1016/j.jhydrol.2015.04.041

Genest, C., Rémillard, B., Beaudoin, D., 2009. Goodness-of-fit tests for copulas: A review and a power study. Insurance: Mathematics and Economics, 44(2): 199-213. https://doi.org/10.1016/j.insmatheco.2007.10.005

Gilroy, K.L., Mccuen, R.H., 2012. A nonstationary flood frequency analysis method to adjust for future climate change and urbanization. Journal of Hydrology, s 414–415(2): 40-48. https://doi.org/10.1016/j.jhydrol.2011.10.009

Graf, W.L., 1999. Dam nation: A geographic census of American dams and their large-scale hydrologic impacts. Water resources research, 35(4): 1305-1311. https://doi.org/10.1029/1999WR900016

Goel, N.K., Kurothe, R.S., Mathur, B.S., Vogel, R.M., 1997. A derived flood frequency distribution for correlated rainfall intensity and duration. Water Resources Research, 33(9): 2103–2107. https://doi.org/10.1029/97WR00812

GUO, W.-x., XIA, Z.-q., WANG, Q., 2008. Effects of Danjiangkou Reservoir on hydrological regimes in the middle and lower reaches of Hanjiang River. Journal of Hohai University (Natural Sciences), 36(6): 733-737. https://doi.org/10.3876/j.issn.1000-1980.2008.06.002

Jiang, C., Xiong, L., Xu, C.Y., Guo, S., 2014. Bivariate frequency analysis of nonstationary low-flow series based on the time-varying copula. Hydrological Processes, 29(6): 1521-1534. https://doi.org/10.1002/hyp.10288

Kwon, H.-H., Brown, C., Lall, U., 2008. Climate informed flood frequency analysis and prediction in Montana using hierarchical Bayesian modeling. Geophysical Research Letters, 35(5). https://doi.org/10.1029/2007GL032220

López, J., Francés, F., 2013. Non-stationary flood frequency analysis in continental Spanish rivers, using climate and reservoir indices as external covariates. Hydrology and Earth System Sciences, 17(8): 3189-3203. https://doi.org/10.5194/hess-17-3189-2013

Lee, J., Heo, J.-H., Lee, J., Kim, N., 2017. Assessment of Flood Frequency Alteration by Dam Construction via SWAT Simulation. Water, 9(4): 264. https://doi.org/10.3390/w9040264

Liang, Z. et al., 2017. A sample reconstruction method based on a modified reservoir index for flood frequency analysis of non-stationary hydrological series. Stochastic Environmental Research and Risk Assessment: 1-11. https://doi.org/10.1007/s00477-017-1465-1

Lu, G.-b., Liu, Y., Zou, X.-l., Zou, Z.-h., Cai, T., 2009. Impact of the Danjiangkou Reservoir on the flow regime in the middle and lower reaches of Hanjiang River. Resources and Environment in the Yangtze Basin, 18(10): 959-963.

Magilligan, F.J., Nislow, K.H., 2005. Changes in hydrologic regime by dams. Geomorphology, 71(1-2): 61-78. https://doi.org/10.1016/j.geomorph.2004.08.017

Martins, E.S., Stedinger, J.R., 2000. Generalized maximum-likelihood generalized extreme-value quantile estimators for hydrologic data. Water Resources Research, 36(3): 737-744. https://doi.org/10.1029/1999WR900330

Martins, E.S., Stedinger, J.R., 2001. Generalized maximum likelihood Pareto-Poisson estimators for partial duration series. Water Resources Research, 37(10): 2551-2557.

Mei, X., Dai, Z., Van Gelder, P.H.A.J.M., and Gao, J., 2015. Linking Three Gorges Dam and downstream hydrological regimes along the Yangtze River, China. Earth and Space Science, 2(4): 94-106. https://doi.org/10.1002/2014EA000052

Milly, P.C.D. et al., 2008. Stationarity Is Dead: Whither Water Management? Science, 319(5863): 573-4. https://doi.org/10.1029/2001WR000367

Nelsen, R., 2006. An Introduction to Copulas . NY: Springer Science+ Business Media. Inc. https://doi.org/10.1007/0-387-28678-0

Ouarda, T., and S. El‐Adlouni (2011), Bayesian nonstationary frequency analysis of hydrological variables 1, JAWRA Journal of the American Water Resources Association, 47(3), 496-505. https://doi.org/10.1111/j.1752-1688.2011.00544.x

Pettitt, A.N., 1979. A Non-Parametric Approach to the Change-Point Problem. Journal of the Royal Statistical Society, 28(2): 126. https://www.jstor.org/stable/2346729

Reis Jr, D.S., Stedinger, J.R., 2005. Bayesian MCMC flood frequency analysis with historical information. Journal of hydrology, 313(1-2): 97-116. https://doi.org/10.1016/j.jhydrol.2005.02.028

Ribatet, M., Sauquet, E., Grésillon, J.-M., Ouarda, T.B., 2007. Usefulness of the reversible jump Markov chain Monte Carlo model in regional flood frequency analysis. Water Resources Research, 43(8). https://doi.org/10.1029/2006WR005525

Rigby, R.A., Stasinopoulos, D.M., 2005. Generalized additive models for location, scale and shape. Appl. Statist., 54(3): 507-554. https://doi.org/10.1111/j.1467-9876.2005.00510.x

Salas, J.D. (1993) Analysis and Modeling of Hydrologic Time Series. In: Maidment, D.R., Ed., Handbook of Hydrology, McGraw-Hill, New York, 19.1-19.72.

Scarf, P., 1992. Estimation for a four parameter generalized extreme value distribution. Communications in Statistics-Theory and Methods, 21(8): 2185-2201. https://doi.org/10.1080/03610929208830906

Schwarz, G., 1978. Estimating the dimension of a model. The Annals of Statistics, 6(2), 461-464.

Sklar, M., 1959. Fonctions de repartition an dimensions et leurs marges. Publications de l'Institut Statistique de l'Université de Paris, 8: 229-231.

Su, C., Chen, X., 2018. Assessing the effects of reservoirs on extreme flows using nonstationary flood frequency models with the modified reservoir index as a covariate. Advances in Water Resources. https://doi.org/10.1016/j.advwatres.2018.12.004

Viglione, A., Merz, R., Salinas, J.L., Blöschl, G., 2013. Flood frequency hydrology: 3. A Bayesian analysis. Water Resources Research, 49(2): 675-692. https://doi.org/10.1029/2011WR010782

Villarini, G. et al., 2009. Flood frequency analysis for nonstationary annual peak records in an urban drainage basin. Advances in Water Resources, 32(8): 1255-1266. https://doi.org/10.1016/j.advwatres.2009.05.003

Volpi, E., Di Lazzaro M., Bertola M., Viglione A., and Fiori A., 2018. Reservoir Effects on Flood Peak Discharge at the Catchment Scale. Water Resources Research, 54(11): 9623-9636. https://doi.org/10.1029/2018WR023866

Wang, W. et al., 2017. Nonlinear filtering effects of reservoirs on flood frequency curves at the regional scale. Water Resources Research, 53(10): 8277-8292. https://doi.org/10.1002/2017WR020871

Wyżga, B., Kundzewicz, Z.W., Ruiz-Villanueva, V., Zawiejska, J., 2016. Flood generation mechanisms and changes in principal drivers, Flood Risk in the Upper Vistula Basin. Springer, pp. 55-75. https://doi.org/10.1007/978-3-319-41923-7_4

Xiong, B., Xiong, L., Chen, J., Chong-Yu, X., Li, L., 2018. Multiple causes of nonstationarity in the Weihe annual low-flow series. Hydrology and Earth System Sciences, 22(2): 1525. https://doi.org/10.5194/hess-22-1525-2018

Xiong, L., Jiang, C., Xu, C.Y., Yu, K.X., Guo, S., 2015. A framework of change-point detection for multivariate hydrological series. Water Resources Research, 51(10): 8198-8217. https://doi.org/10.1002/2015WR017677

Yan, L., Xiong, L., Liu, D., Hu, T., Xu, C.Y., 2017. Frequency analysis of nonstationary annual maximum flood series using the time-varying two-component mixture distributions. Hydrological Processes, 31(1): 69-89. https://doi.org/10.1002/hyp.10965

Yang, T., Zhang Q., Chen Y.D., Tao X., Xu C.Y., and Chen X., 2008. A spatial assessment of hydrologic alteration caused by dam construction in the middle and lower Yellow River, China. Hydrological Processes: An International Journal, 22(18): 3829-3843. https://doi.org/10.1002/hyp.6993

Zhang L., Xu J., Huo, J., Chen J., 2009. Study on Stage Flood Control Water Level of Danjiangkou Reservoir. Journal of Yangtze River Scientific Research Institute, 26 (3): 13-14. (In Chinese)

Zhang, Q., Gu, X., Singh, V.P., Xiao, M., Chen, X., 2015. Evaluation of flood frequency under non-stationarity resulting from climate indices and reservoir indices in the East River basin, China. Journal of Hydrology, 527: 565-575. https://doi.org/10.1016/j.jhydrol.2015.05.029

Tables

Table 1. Summary of the probability density functions, the corresponding moments and the used link functions for nonstationary flood frequency analysis.

Distributions	Probability density functions	Moments	Link functions
Gamma (GA)	$f_Y\left(y\vert\mu_t,\sigma_t\right)=\frac{\left(y\right)^{1/\sigma_t^2-1}}{\Gamma\left(1/\sigma_t^2\right)\left(\mu\sigma_t^2\right)^{1/\sigma_t^2}}\exp\left(-\frac{y}{\mu_t\sigma_t^2}\right)$ $y>0,\mu_t>0,\sigma_t>0$	$E\left(Y\right)=\mu_t$ $Var\left(Y\right)=\mu_t^2\sigma_t^2$	$g_1\left(\mu_t\right)=\ln\left(\mu_t\right)$ $g_2\left(\sigma_t\right)=\ln\left(\sigma_t\right)$
Weibull (WEI)	$f_Y\left(y\vert\mu_t,\sigma_t\right)=\left(\frac{\sigma_t}{\mu_t}\right)\left(\frac{y}{\mu_t}\right)^{\sigma_t-1}\exp\left(-\left(\frac{y}{\mu_t}\right)^{\sigma_t}\right)$ $y>0,\mu_t>0,\sigma_t>0$	$E\left(Y\right)=\mu_t\Gamma\left(1+1/\sigma_t\right)$ $Var\left(Y\right)=\mu_t^2\left[\Gamma\left(1+2/\sigma_t\right)-\Gamma^2\left(1+1/\sigma_t\right)\right]$	$g_1\left(\mu_t\right)=\ln\left(\mu_t\right)$ $g_2\left(\sigma_t\right)=\ln\left(\sigma_t\right)$
Lognormal (LOGNO)	$f_Y\left(y\vert\mu_t,\sigma_t\right)=\frac{1}{y\sigma_t\sqrt{2\pi}}\exp\left\{-\frac{\left[\log\left(y\right)-\mu_t\right]^2}{2\sigma_t^2}\right\}$ $y>0,-\infty<\mu_t<\infty,\sigma_t>0$	$E\left(Y\right)=w^{1/2}\exp(\mu_t)$ $Var\left(Y\right)=w(w-1)\exp(2\mu_t)$ $w=\exp(\sigma_t^2)$	$g_1\left(\mu_t\right)=\ln\left(\mu_t\right)$ $g_2\left(\sigma_t\right)=\ln\left(\sigma_t\right)$
Gumbel (GU)	$f_Y\left(y\vert\mu_t,\sigma_t\right)=\frac{1}{\sigma_t}\exp\left\{\left(\frac{y-\mu_t}{\sigma_t}\right)-\exp\left(\frac{y-\mu_t}{\sigma_t}\right)\right\}$ $-\infty<y<\infty,-\infty<\mu_t<\infty,\sigma_t>0$	$E\left(Y\right)=\mu_t-0.57722\sigma_t$ $Var\left(Y\right)=\left(\pi^2/6\right)\sigma_t^2$	$g_1\left(\mu_t\right)=\mu_t$ $g_2\left(\sigma_t\right)=\ln\left(\sigma_t\right)$
Generalized Extreme Value (GEV)	$f_Y\left(y\vert\mu_t,\sigma_t,\xi\right)=\frac{1}{\sigma_t}\left[1+\xi\left(\frac{y-\mu_t}{\sigma_t}\right)\right]^{-1/\xi-1}\exp\left\{-\left[1+\xi\left(\frac{y-\mu_t}{\sigma_t}\right)\right]^{-1/\xi}\right\}$ $y>\mu_t-\sigma_t/\xi,-\infty<\mu_t<\infty,\sigma_t>0,-\infty<\xi<\infty$	$E\left(Y\right)=\mu_t-\frac{\sigma_t}{\xi}+\frac{\sigma_t}{\xi}\eta_1$ $Var\left(Y\right)=\sigma_t^2\left(\eta_2-\eta_1^2\right)/\xi$ $\eta_m=\Gamma\left(1-m\xi\right)$	$g_1\left(\mu_t\right)=\mu_t$ $g_2\left(\sigma_t\right)=\ln\left(\sigma_t\right)$

Table 2. Seven nonstationary scenarios for the formulas of the two distribution parameters (i.e., μ_t and σ_t).

Scenario classification	Scenario codes	The formula of distribution parameters	
		$g_1(\mu_t)$	$g_2(\sigma_t)$
Stationary (S0)	S0	α_0	β_0
RI-dependent (S1)	S11	$\alpha_0+\alpha_1$RI	β_0
	S12	α_0	$\beta_0+\beta_1$RI
	S13	$\alpha_0+\alpha_1$RI	$\beta_0+\beta_1$RI
RRCI-dependent (S2)	S21	$\alpha_0+\alpha_1$RRCI	β_0
	S22	α_0	$\beta_0+\beta_1$RRCI
	S23	$\alpha_0+\alpha_1$RRCI	$\beta_0+\beta_1$RRCI

Table 3. Information of the five major reservoirs in Hanjiang River basin.

Reservoirs	Longitude	Latitude	Area (km^2)	Year	Capacity (10^9 m^3)
Shiquan	108.05	33.04	23400	1974	0.566
Ankang	108.83	32.54	35700	1992	3.21
Huanglongtan	110.53	32.68	10688	1978	1.17
Dangjiangkou	111.51	32.54	95220	1967	34.0
Yahekou	112.49	33.38	3030	1960	1.32

Table 4. Change in the mean and standard deviation of AMDF after the construction of the two large reservoirs (i.e., Danjiangkou reservoir completed by 1967, and Ankang reservoir built by 1992).

Stations	Mean (m^3/s)			Standard deviation (m^3/s)		
	1956-1966	1967-1991	1992-2015	1956-1966	1967-1991	1992-2015
AK	9451	10468	6506	4341	4623	4454
HJG	14951	7524	4139	7896	5482	4074
HZ	16603	10120	5958	8833	5420	4721

Table 5. Correlation coefficients between RRCI and AMDF.

Subset of rainfall variables	AK			HJG			HZ		
	Pearson	Kendall	Spearman	Pearson	Kendall	Spearman	Pearson	Kendall	Spearman
-*	-0.37	-0.18	-0.28	-0.55	-0.37	-0.54	-0.53	-0.38	-0.55
M	-0.27	-0.27	-0.37	-0.67	-0.53	-0.74	-0.45	-0.37	-0.51
I	-0.26	-0.25	-0.34	**-0.74**	-0.57	-0.79	-0.54	-0.41	-0.56
V	-0.32	-0.28	-0.39	-0.63	-0.49	-0.69	-0.57	-0.48	-0.65
T	-0.11	-0.17	-0.24	-0.68	-0.55	-0.73	-0.48	-0.40	-0.57
M, *I*	-0.37	-0.28	-0.38	-0.70	-0.56	-0.77	-0.56	-0.43	-0.58
M, *V*	-0.42	-0.29	-0.40	-0.64	-0.50	-0.71	-0.56	-0.45	-0.60
M, *T*	-0.37	-0.26	-0.36	-0.69	-0.57	-0.77	-0.64	-0.46	-0.63
I, *V*	-0.46	-0.31	-0.42	-0.71	-0.54	-0.76	-0.65	-0.50	-0.67
I, *T*	-0.34	-0.22	-0.31	-0.73	**-0.60**	**-0.80**	-0.68	-0.50	-0.66
V, *T*	-0.43	-0.28	-0.39	-0.68	-0.55	-0.75	-0.69	-0.52	-0.71
M, *I*, *V*	-0.49	-0.31	-0.42	-0.65	-0.53	-0.74	-0.63	-0.47	-0.63
M, *I*, *T*	-0.41	-0.27	-0.37	-0.68	-0.57	-0.78	-0.67	-0.49	-0.66
M, *V*, *T*	-0.50	-0.29	-0.40	-0.65	-0.56	-0.76	-0.67	-0.49	-0.67
I, *V*, *T*	-0.51	-0.31	-0.41	-0.67	-0.58	-0.78	**-0.71**	**-0.53**	**-0.70**
M, *I*, *V*, *T*	**-0.53**	**-0.31**	**-0.42**	-0.65	-0.57	-0.77	-0.69	-0.52	-0.69

*The values in the first row are the correlation coefficients between RI and flood series

Table 6. Results of copula models for scheduling-related rainfall variables.

Stations	Scheduling-related variables	Pairs	Copula type	Parameters θ_c	Kendall's tau	Goodness-of-fit test based on the empirical copula	
						CvM*	p-value
AK	*M*, *I*, *V*, *T*	14	Clayton	0.16	0.08	0.169	0.860
		13	Clayton	1.28	0.39		
		12	Clayton	1.01	0.33		
		24|1	Frank	1.21	0.17		
		23|1	Frank	-2.24	-0.24		
		34|12	Clayton	0.96	0.11		
HJG	*I*, *T*	24	Clayton	1.37	0.41	0.473	0.425
HZ	*I*, *V*, *T*	24	Gumbel	1.12	0.11	0.181	0.820
		23	Clayton	1.31	0.40		
		34|2	Clayton	0.49	0.20		

* CvM is the statistic of the Cramer-von Mises test; if the p-value of the C-vine copula model is less than the significance level of 0.05, the model is considered to be not consistent with the empirical copula.

Table 7. Summary of results of the nonstationary flood distribution models.

Stations	Covariates	Distributions	The optimal formulas* of distribution parameters				AIC	SBC
			Selected models	μ_t	σ_t	ξ		
AK	RI	GA	WEI_S23	exp(9.24-2.64RI)	exp(-0.769+2.9RI)	-	1177.2	1185.5
	RI	WEI		exp(9.36-2.83RI)	exp(0.882-3.18RI)	-	1176.9	1185.3
	RI	LOGNO		exp(9.14-3.86RI)	exp(-0.716+3.28RI)	-	1180.4	1188.8
	RI	GU		11875-13093RI	exp(8.5)	-	1199.6	1205.9
	RI	GEV		7685-15252RI	exp(8.3)	-0.043	1182.3	1190.6
	RRCI	GA		exp(9.28-1.11RRCI)	exp(-0.825+0.689RRCI)	-	1165.3	1173.7
	RRCI	WEI		exp(9.4-1.17RRCI)	exp(0.982-0.884RRCI)	-	1163.8	**1172.2**
	RRCI	LOGNO		exp(9.19-1.33RRCI)	exp(-0.749+0.677RRCI)	-	1168.0	1176.4
	RRCI	GU		12555-7535RRCI	exp(8.4)	-	1188.0	1194.2
	RRCI	GEV		8460-6722RRCI	exp(8.2)	-0.096	1172.1	1180.5
HJG	RI	GA	GA_S21	exp(9.7-1.62RI)	exp(-0.25)	-	1139.9	1146.0
	RI	WEI		exp(9.75-1.56RI)	exp(0.27)	-	1141.4	1147.5
	RI	LOGNO		exp(9.47-1.8RI)	exp(-0.17)	-	1140.9	1147.1
	RI	GU		17955-14399RI	exp(8.8)	-	1189.5	1195.7
	RI	GEV		6976-5930RI	exp(8.79-1.49RI)	0.43	1149.9	1160.2
	RRCI	GA		exp(9.99-1.99RRCI)	exp(-0.45)	-	1112.5	**1118.6**
	RRCI	WEI		exp(10.1-1.97RRCI)	exp(0.53)	-	1113.2	1119.4
	RRCI	LOGNO		exp(9.75-1.94RRCI)	exp(-0.38)	-	1113.9	1120.1
	RRCI	GU		23067-20871RRCI	exp(9.2-1.7RRCI)	-	1121.3	1129.6
	RRCI	GEV		12113-10683RRCI	exp(9.2-2.01RRCI)	0.051	1112.5	1122.8
HZ	RI	GA	WEI_S21	exp(9.85-2.87RI)	exp(-0.42)	-	1198.3	1204.9
	RI	WEI		exp(9.94-2.79RI)	exp(0.49)	-	1198.6	1204.9
	RI	LOGNO		exp(9.63-2.93RI)	exp(-0.33)	-	1201.1	1207.4
	RI	GU		18661-23706RI	exp(8.8)	-	1237.5	1243.7
	RI	GEV		9605-13545RI	exp(9.03-2.56RI)	0.099	1207.8	1218.3
	RRCI	GA		exp(9.85-1.52RRCI)	exp(-0.61)	-	1173.1	1179.4
	RRCI	WEI		exp(9.92-1.42RRCI)	exp(0.73)	-	1171.2	**1177.5**
	RRCI	LOGNO		exp(9.72-1.55RRCI)	exp(-0.51)	-	1178.7	1185.0
	RRCI	GU		19214-14344RRCI	exp(8.86-0.881RRCI)	-	1189.7	1198.1
	RRCI	GEV		12502-9911RRCI	exp(8.96-1.37RRCI)	-0.068	1176.0	1186.4

*The model parameters in the optimal formulas are the posterior mean from Bayesian inference.

Table 8. Summary of the rainfall information for the five largest floods after the construction (1967) of Danjiangkou reservoir in HZ station.

Year	Values (Ranking in 1967-2015)				
	AMDF [m^3/s]	OR_JEP [-]	I [mm]	V [mm]	T [day of the year]
1983	25600 (1)	0.435 (2)	20.2 (1)	121.4 (19)	281 (2)
1975	19900 (2)	0.557 (7)	9.6 (18)	163.6 (13)	277 (6)
1974	18200 (3)	0.506 (4)	12.0 (7)	120.4 (20)	278 (4)
2005	16800 (4)	0.651 (11)	8.2 (27)	179.7 (10)	278 (4)
1984	16100 (5)	0.461 (3)	9.9 (15)	256.3 (4)	273 (9)

Figures

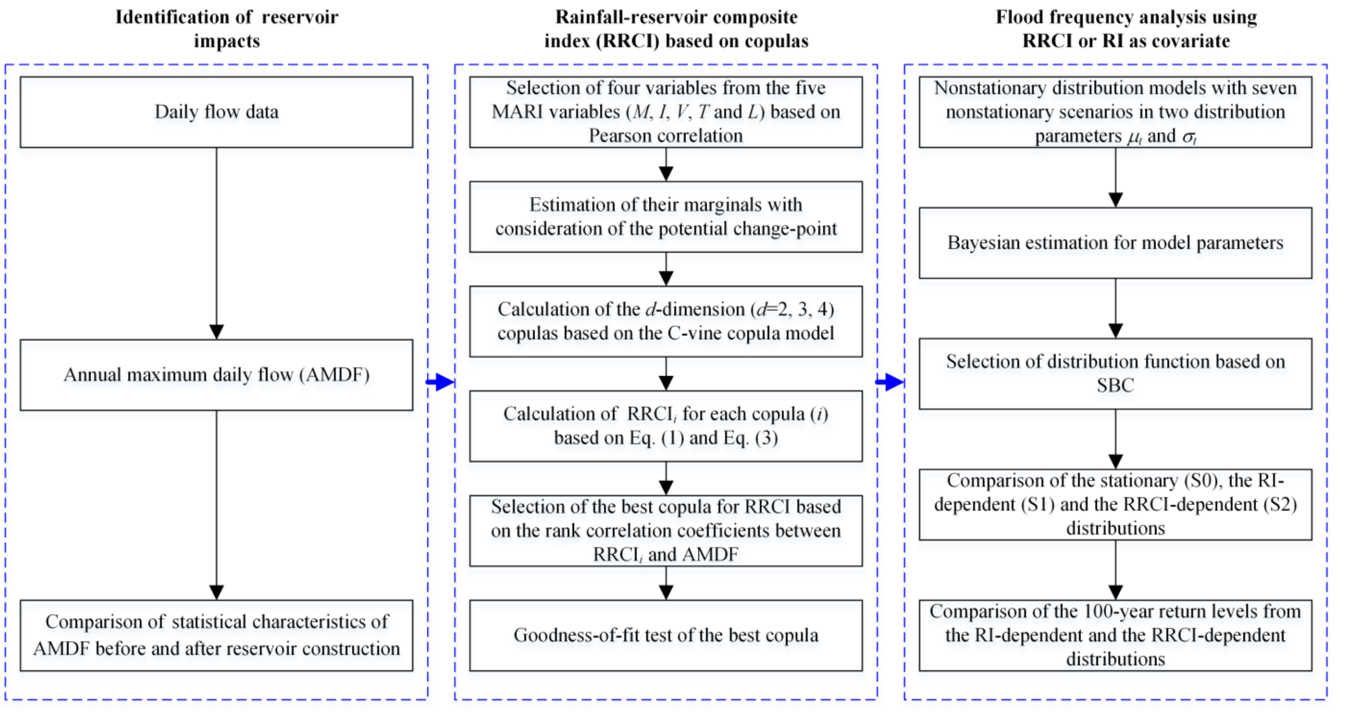

Figure 1. Flowchart of nonstationary covariate-based flood frequency analysis with a rainfall-reservoir composite index (RRCI).

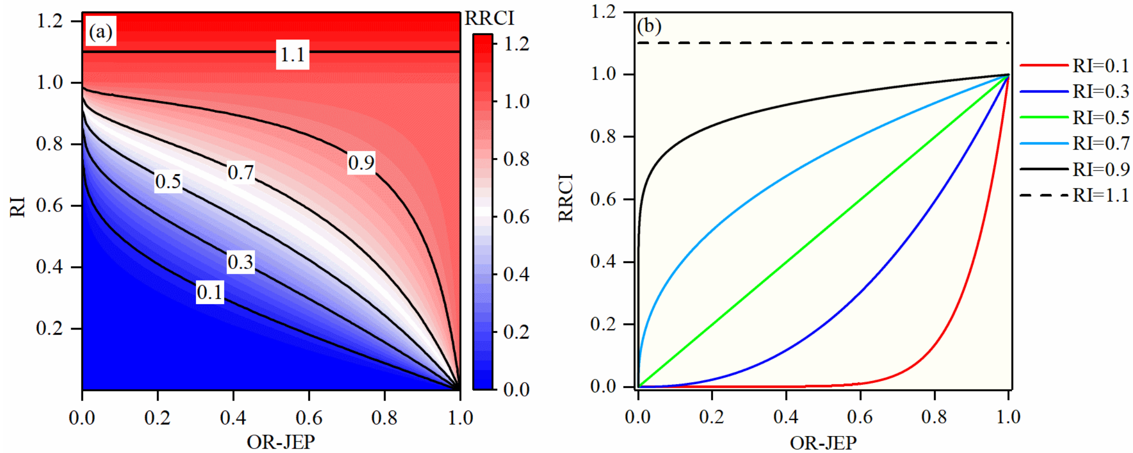

Figure 2. Relationship in the Eq. (2). (a) is the contour plot of RRCI against both RI and OR-JEP; (b) is the function curves of RRCI against OR-JEP under the different values of RI.

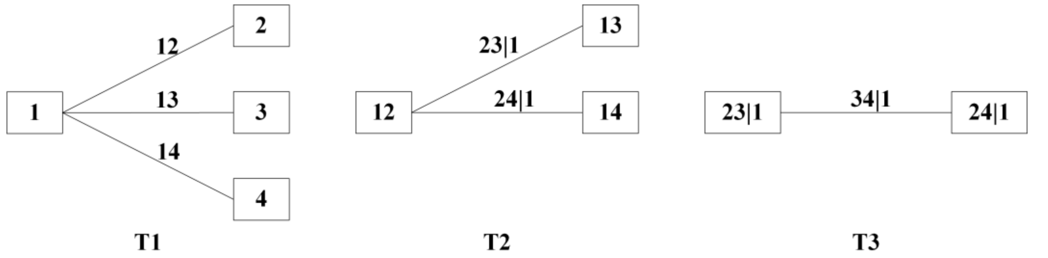

Figure 3. Decomposition of a C-vine copula with four variables and 3 trees (denoted by T1, T2 and T3).

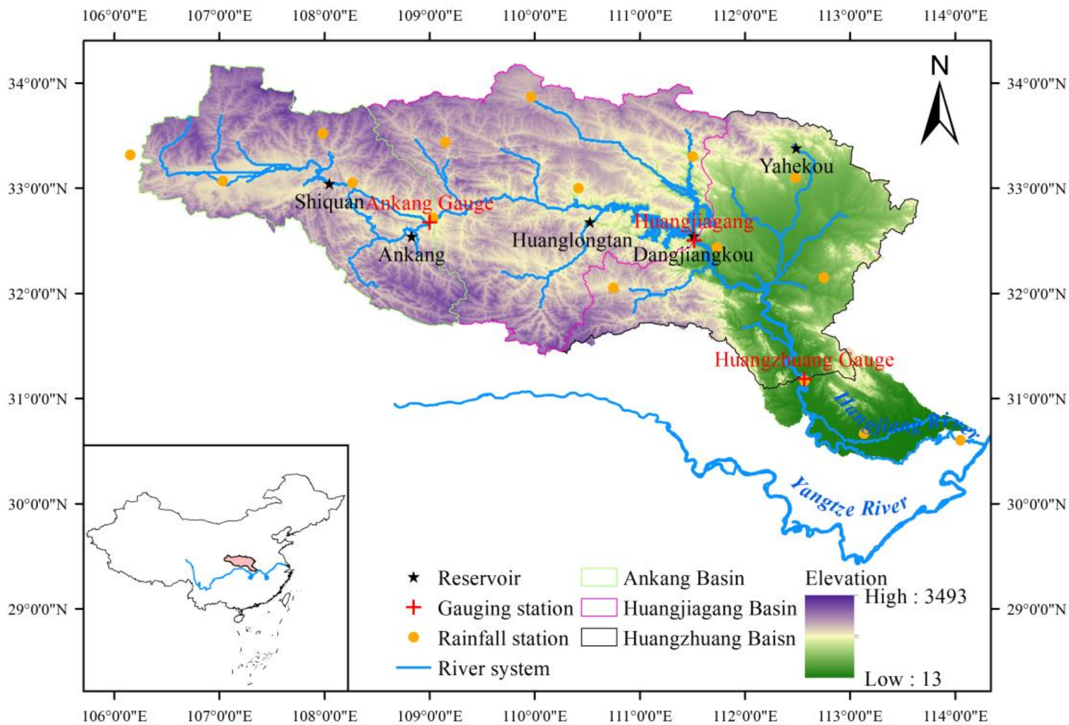

Figure 4. Geographic location of the reservoirs, gauging stations and rainfall stations in Hanjiang River.

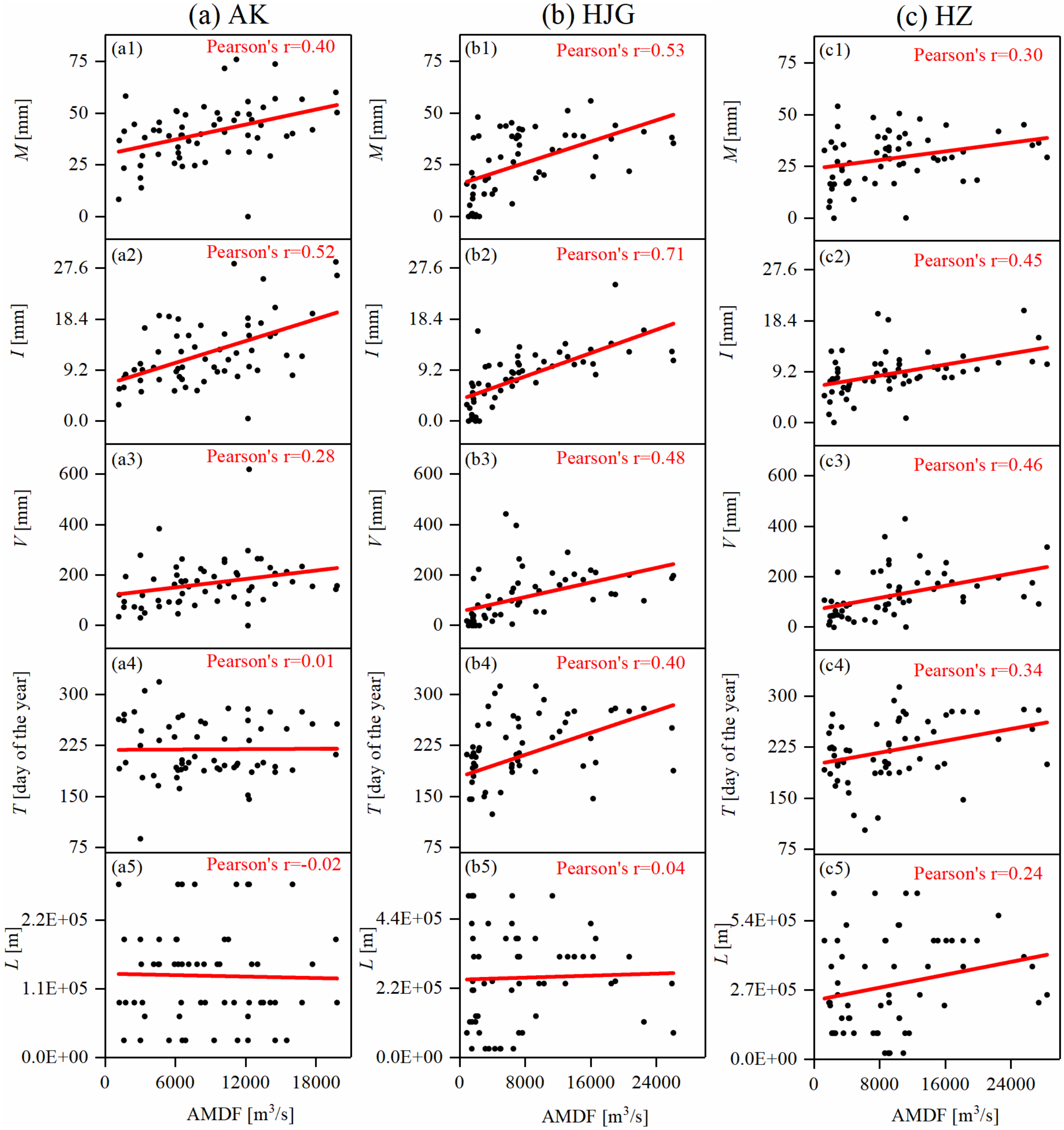

Figure 5. Linear correlation between the five MARI variables and AMDF for (a) AK station, (b) HJG station and (c) HZ station.

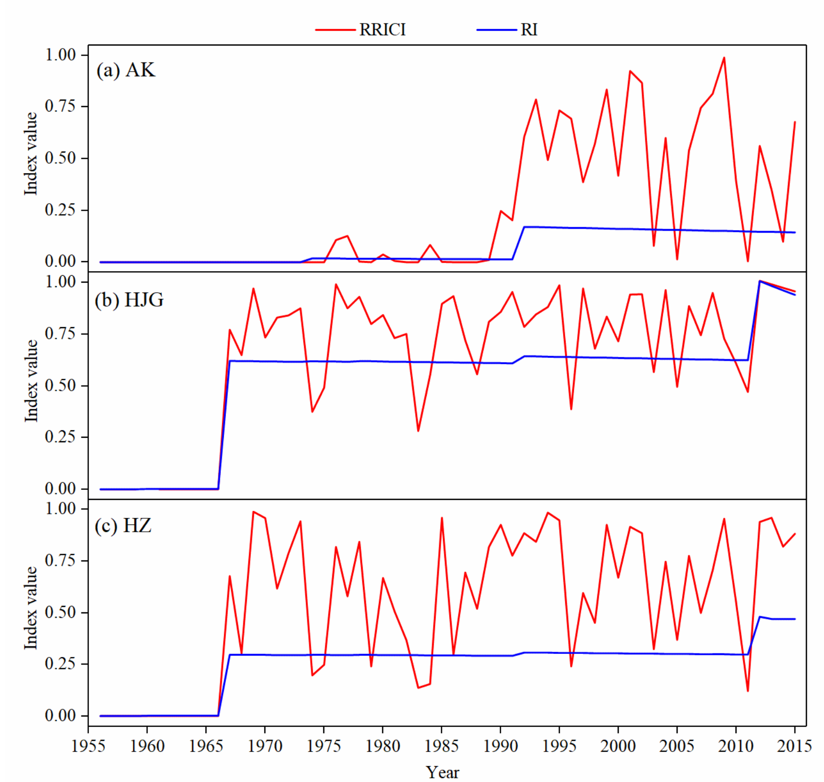

Figure 6. Variation of RI and RRCI for (a) AK station, (b) HJG station and (c) HZ station.

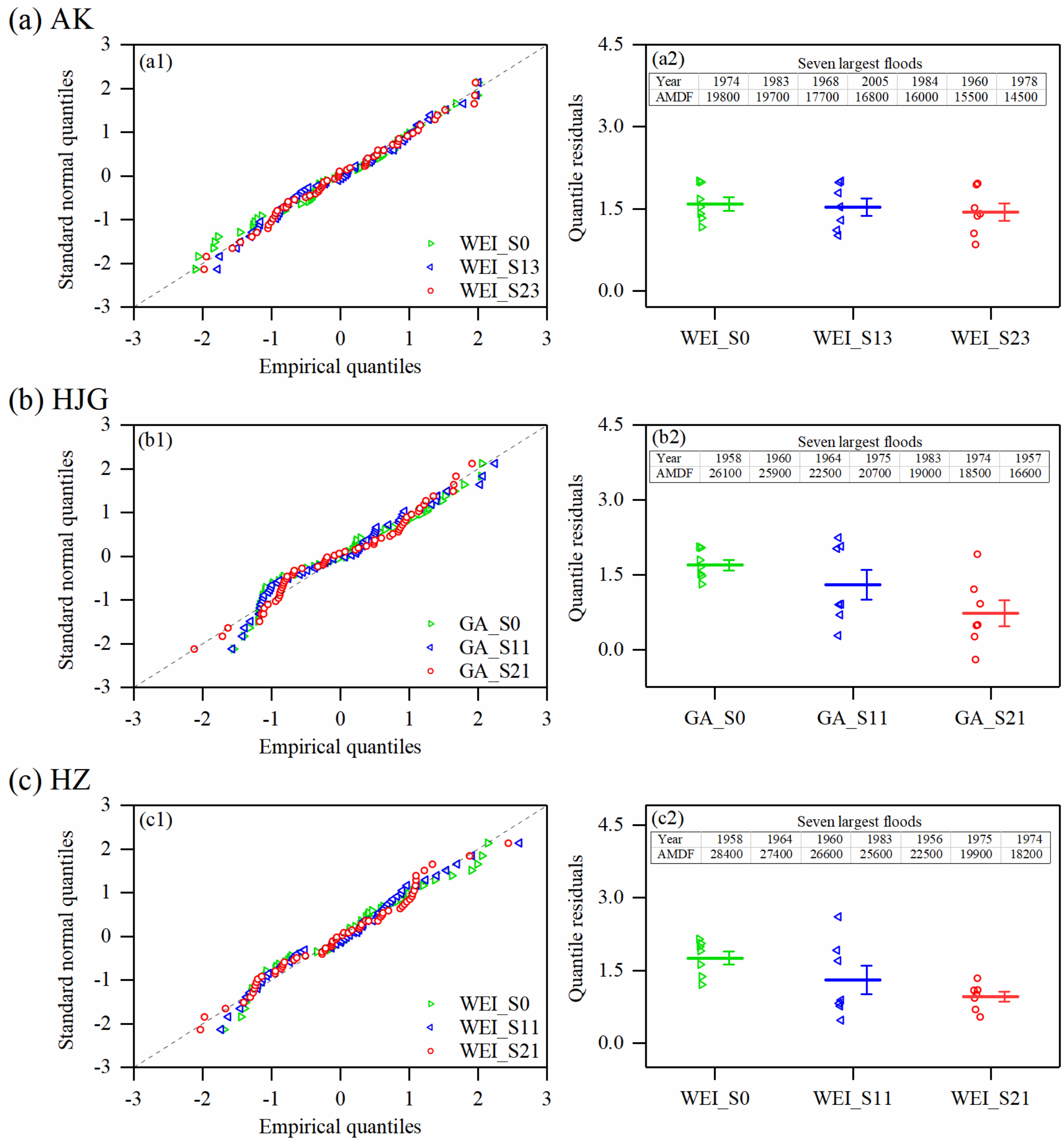

Figure 7. Comparison of the stationary (S0), the RI-dependent (S1) and the RRCI-dependent (S2) scenarios of the same optimal distributions for (a) AK station, (b) HJG station and (c) HZ station. The left panels (a1, b1 and c1) are the QQ plots for the whole AMDF series in each station. The right panels (a2, b2 and c2) are the plots of quantile residuals for the seven largest floods (their values and

occurrence years have been listed) in each station, and the means of their quantile residuals (points) and the corresponding standard errors are indicated by the lines.

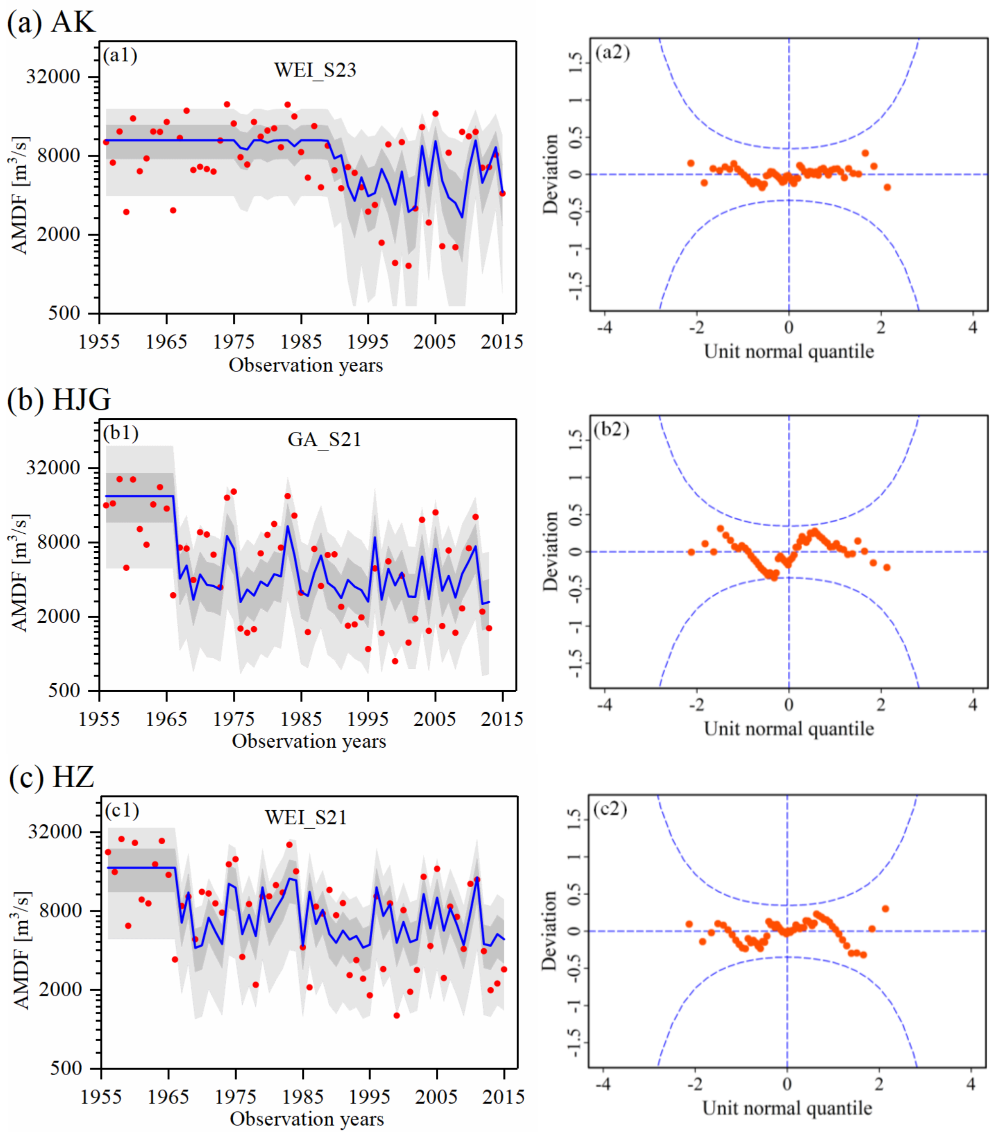

Figure 8. Performance of (a) WEI_S23 for AK station, (b) GA_S21 for HJG station and (c) WEI_S21 for HZ station. The left panels (a1, b1 and c1) are the centile curves plots in each station (the 50th centile curves are indicated by the thick blue lines; the light gray-filled areas are between the 5th and 95th centile curves; the dark grey-filled areas are between the 25th and 75th centile curves; the

filled red points indicate the observed series). The right panels (a2, b2 and c2) are the worm plots; a reasonable model should have the plotted points within the 95% confidence intervals (between the two blue dashed curves).

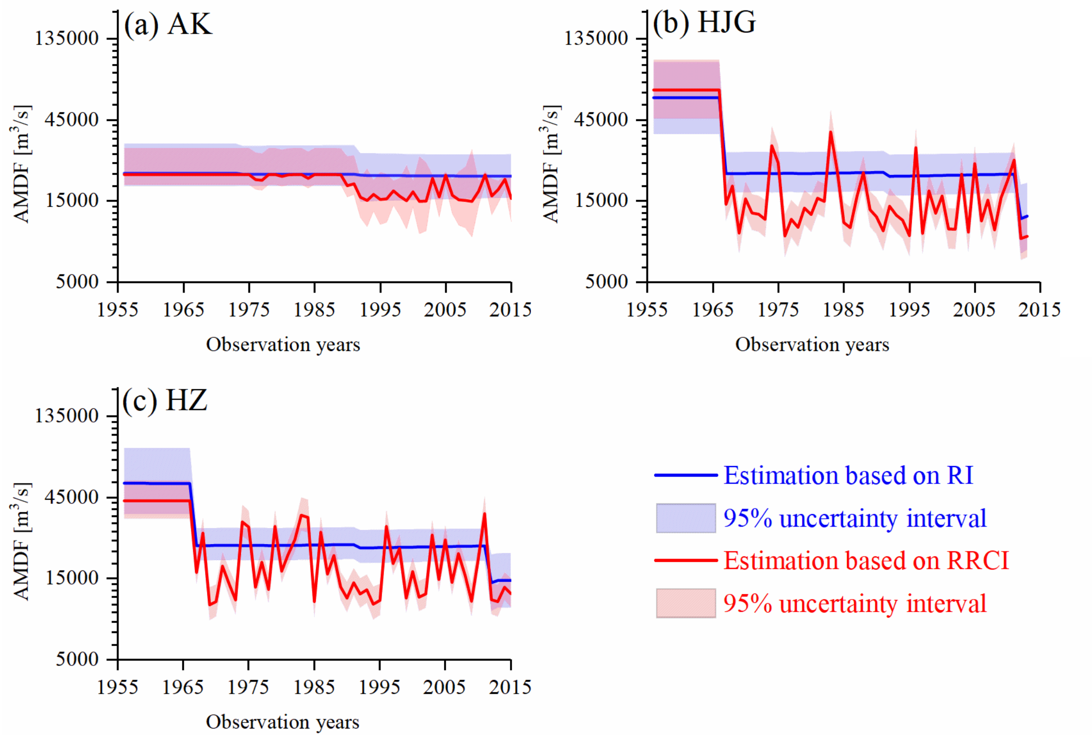

Figure 9. Statistical inference of the 100-year return levels with the 95% uncertainty interval using the optimal RI-dependent and RRCI-dependent distributions: (a) WEI_S13 and WEI_S23 for AK station, (b) GA_11 and GA_S21 for HJG station, and (c) WEI_S11 and WEI_S21 for HZ station.